Electronic supplementary information

Modular interior loading and exterior decoration of a Virus-like particle

Jhanvi Sharma,[a] Masaki Uchida,[a] Heini M. Miettinen,[b] and Trevor Douglas*[a]

[a] Department of Chemistry, Indiana University, 800 East Kirkwood Avenue, Bloomington, Indiana 47405, United States
[b] Department of Microbiology and Immunology, Montana State University, PO Box 173520, Bozeman, Montana 59717, United States
*Email: trevdoug@indiana.edu

Purification and characterization of *in vivo* assembled P22-StAv

Characterization of *in vivo* assembled SEC purified capsids by SDS-PAGE showed two bands corresponding to CP (~47 kDa) and StAv-SP (~35 kDa) confirming the encapsulation of StAv (Figure S1A). The capsids were subsequently analyzed by SEC-MALS/QELS (Figure S1B). SEC-MALS revealed an average molecular weight of 31.6 ± 0.2 MDa, which corresponds to a loading of approximately 338 copies of StAv subunits. The size of the particles, determined by MALS and QELS (R_g = 26.4 ± 0.3 nm) (R_h = 27.9 ± 0.1 nm) matched with those previously reported for encapsulated P22 materials. Transmission electron microscopy (TEM) confirmed that encapsulation did not alter the cage architecture, and that the size of assembled P22-StAv particles (R= 26.5 ± 1.3 nm) were consistent with T=7 P22 particles (Figure S1C). Binding activity of encapsulated StAv was assayed by cumulative titration of StAv with Biotin-4-fluorescein (B4F). The binding of B4F to StAv accompanies with a significant change in molar extinction coefficient of B4F at 493 nm, resulting which a decreased absorbance at that wavelength is observed.[1] Commercial streptavidin was titrated as positive control and PBS was used as negative control. With PBS, the absorbance was increased linearly with a constant slope throughout the successive additions of B4F, whereas in commercial StAv, reduction in absorbance was observed until all binding sites became saturated with B4F. Further addition of B4F resulted in an increase in absorbance with a slope similar to the control experiment, indicating absence of non-specific binding. The data was plotted between absorbance and molar ratio of [B4F]/[StAv subunit] and fitted with a user-defined piecewise linear regression function in Igor pro 6.37. The breakpoint at molar ratio of [B4F]/[StAv subunit] = 1 indicated the binding stoichiometry of StAv to B4F, and that all sites are functional, and in agreement with the specifications provided by the vendor.

To measure binding activity of the StAv in P22-StAv, the concentration of encapsulated StAv was calculated from the absorbance at 280 nm using a molar extinction coefficient of 215, 000 $M^{-1}cm^{-1}$. Details on the determination of molar extinction coefficient is provided later in supplementary information.

Electronic supplementary information

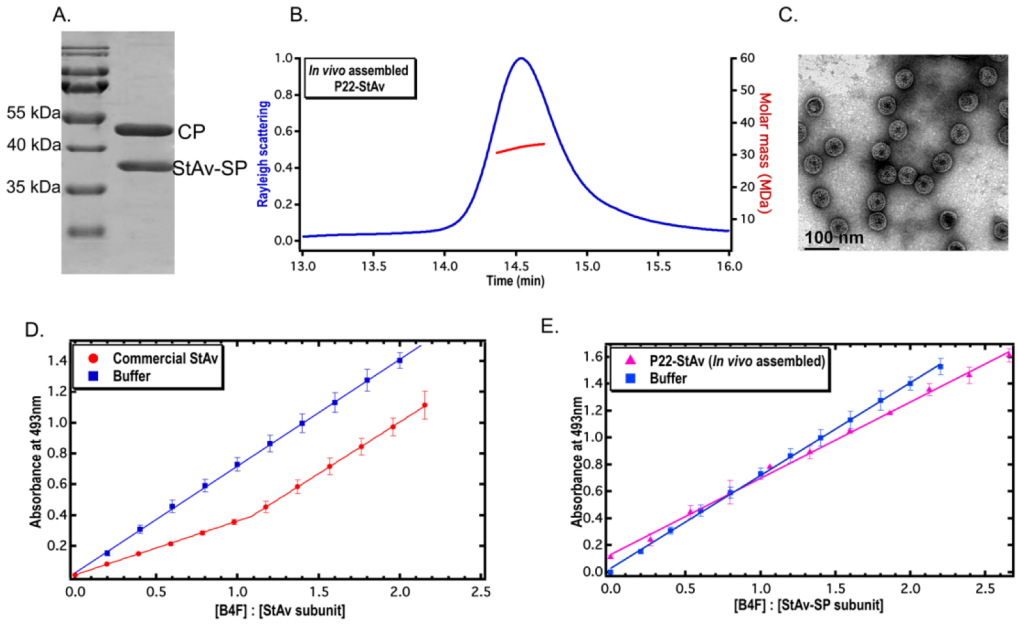

Figure S1.(A) SDS-PAGE analysis of purified P22-StAv shows the band corresponding to CP (~47 kDa) and StAv-SP (~35 kDa). (B) SEC-MALS analysis shows Rayleigh scattering (blue trace) of particles and the distribution of particles weight (MW) across that peak (red trace). (C) TEM image shows monodisperse population and spherical morphology. (D) Binding activity of commercial StAv and PBS Buffer (negative control). Binding of biotin-4-fluorescein (B4F) to StAv results in reduction of the B4F absorbance at 493 nm until all sites are saturated, after which slope changes and becomes parallel to control, indicating no non-specific binding. Commercial StAv shows binding activity with break point occurring at molar ratio of 1, indicating 1:1 binding stoichiometry to B4F. (E). While P22-StAv does not show any change in slope and is therefore functionally inactive. The data were fit with a user-defined piecewise linear regression function. Error bars shows standard deviation of the mean.

Binding activity of *in vivo* assembled P22-StAv particles expressed with chaperones

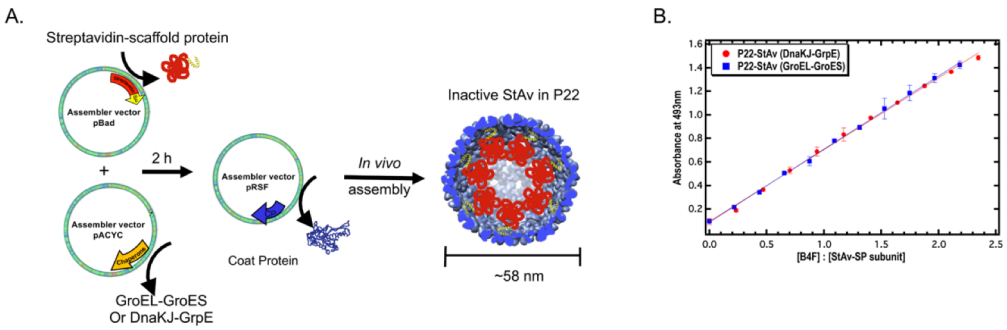

Figure S2. (A) Schematic showing *in vivo* expression and assembly of P22-StAv particles in presence of chaperone system. The StAv-SP and chaperone (DnaKJ-GrpE or GroEL-GroES) was co-expressed together, induced with L-arabinose for 2 h, followed by the CP expression, induced with isopropyl β-D-1-thiogalactopyranoside (IPTG) for 2 h. The assembled particles were isolated, purified and characterized. (B). Binding activity of P22-StAv particles. No change in slope indicates that particles were inactive.

Electronic supplementary information

Purification and characterization of StAv-SP

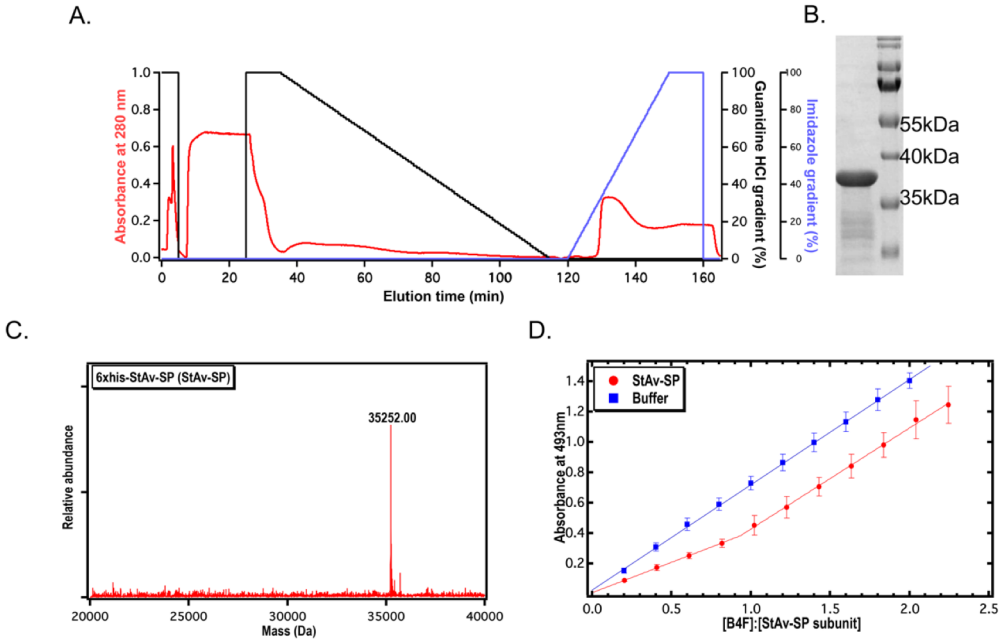

Figure S3. (A) Ni-affinity purification of StAv-SP. The black line shows the linear reverse gradient (6 M – 0 M) of GuHCl and the blue line shows a linear forward gradient of imidazole (20 mM - 500 mM). (B) SDS-PAGE analysis of pooled fractions, eluted between 120 and 140 min, shows the band at expected molecular weight (~35kDa) and indicates the purity of StAv-SP. (C) Mass-spectrometry of StAv-SP reveals the MW of 35,252 Da, which matched well with the expected MW (35,253 Da). (D) Binding activity of refolded StAv-SP. The StAv was titrated with increasing B4F concentration. The change in slope during titration indicates the activity and 1:1 binding stoichiometry of StAv-SP subunit to B4F.

Size distribution of *in vivo* and *in vitro* assembled P22-StAv particles by TEM

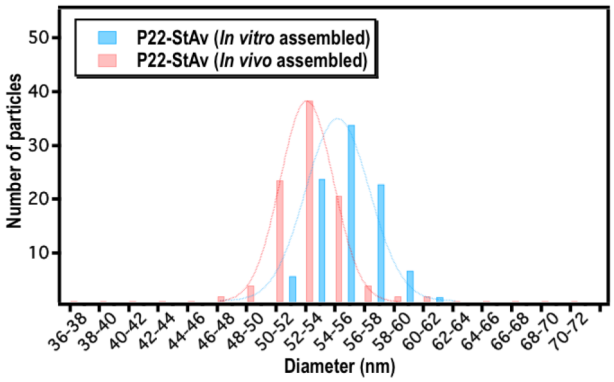

Figure S4. Size distribution determined by statistical analysis of P22-StAv particles in TEM images. Approximately 90 particles were analyzed, and the average particle size of 55.0 ± 3.1 nm and 53.0 ± 2.6 nm was observed for *in vitro* and *in vivo* assembled particles, respectively.

Electronic supplementary information

Non-cumulative titration of *in vitro* assembled P22-StAv particles

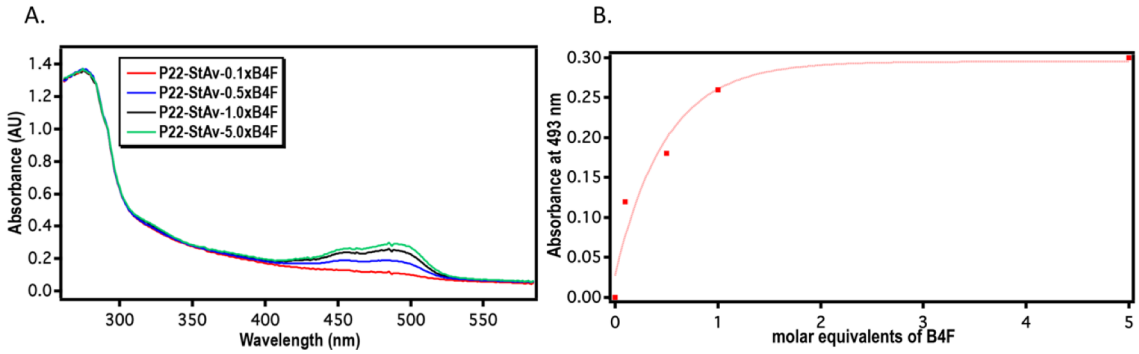

Figure S5. (A). UV-Vis spectroscopy of purified P22-StAv particles that were titrated with B4F, non-cumulatively. (B) The plotted curve shows absorbance values at 493 nm from UV/Vis graph vs. molar equivalents of B4F added to each titration reaction. The curve shows concentration dependent increase in absorbance at 493 nm, which plateaus at excess [B4F] indicating saturation of all binding sites.

Investigation of presaturation of StAv with biotin *in vivo* assembled P22-StAv particles

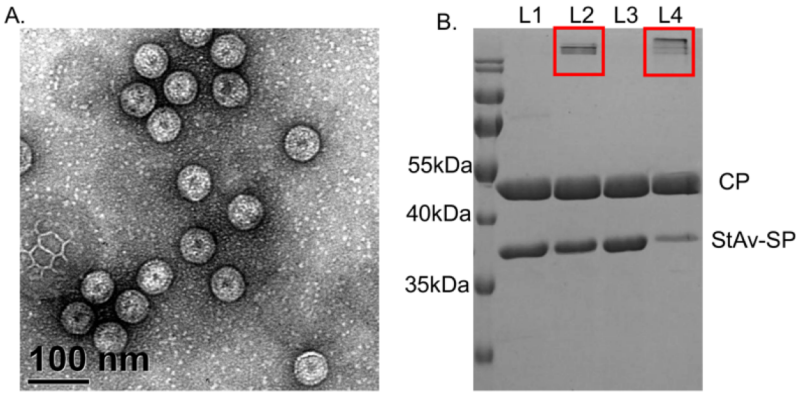

Figure S6. (A) TEM of assembled particles shows intact morphology and monodisperse population. (B) SDS-PAGE analysis of *in vivo* assembled particles (L1), *in vitro* assembled particles (L3), *in vitro* assembled with StAv-SP presaturated with biotin (L2) and *in vitro* assembled with StAv-SP presaturated with B4F (L4). The SDS-PAGE analysis shows encapsulation of presaturated StAv. The high molecular weight bands in lanes L2 and L4 (highlighted in red box) are likely aggregates or oligomers of streptavidin tetramers formed in presence of biotin.[2] These bands are diagnostic for the biotin bound StAv and were not observed in the *in vivo* assembled P22-StAv particles suggesting that available binding sites were not pre-saturated with biotin.

Electronic supplementary information

Densitometric analysis of co-assembled particles run on SDS-PAGE for controlled loading experiments

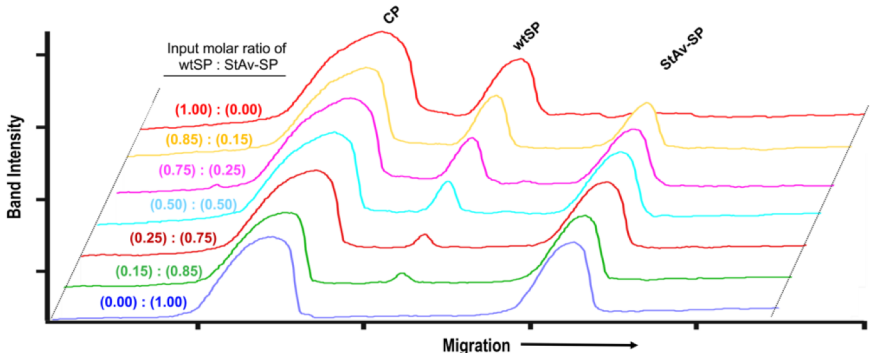

Figure S7. Line-scan densitometry profile of isolated co-assembled particles (L4, L5, L6, L7, L8, L9, 10) run on SDS-PAGE. The profile shows that the amount of encapsulated StAv-SP and wtSP changes as input stoichiometry ratio of these two components changes.

Densitometric analysis of standards run on SDS-PAGE for controlled loading experiments

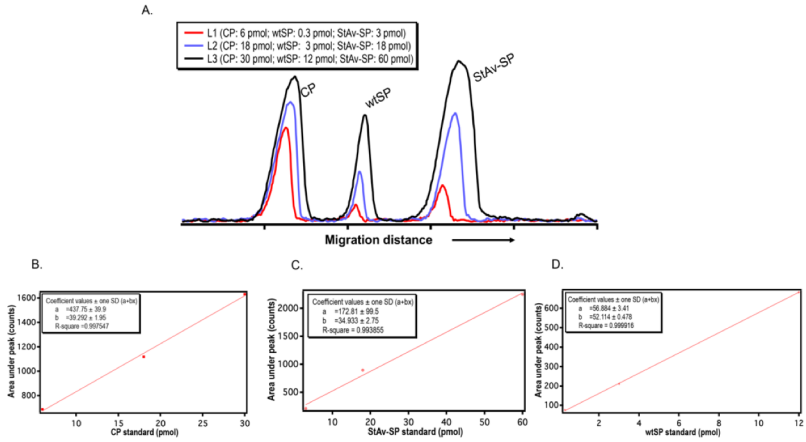

Figure S8. (A) Line-scan densitometry profile of standards (L1, L2, and L3) that contained mixture of CP, wtSP and StAv-SP. (B) Calibration curve of each standard plotted between area under the peak (counts) and concentration (pmol).

Electronic supplementary information

Table S1. Input/output mole ratio of wtSP and StAv-SP in isolated co-assembled capsids

Sample	Input mole ratio of wtSP	Output mole ratio of wtSP	Input mole ratio of StAv-SP	Output mole ratio of StAv-SP
1	1	1	0	0
2	0.85	0.43	0.15	0.57
3	0.75	0.25	0.25	0.75
4	0.5	0.12	0.5	0.88
5	0.25	0.03	0.75	0.96
6	0.15	0.03	0.85	0.96
7	0	0	1	1

Selective release of wtSP from co-assembled capsids using GuHCl

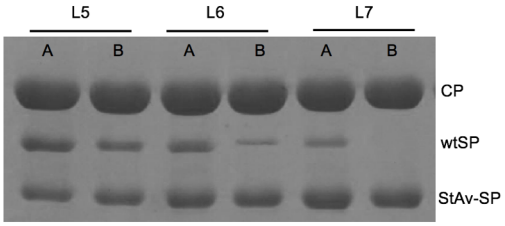

Figure S9. SDS-PAGE analysis of co-assembled capsids before and after 0.5M GuHCl treatment. A and B refers to before and after GuHCl treatment, respectively. L5, L6, and L7 are the co-assembled capsids with different composition of wtSP and StAv-SP.

SDS-PAGE analysis to determine bound copies of B-SP-GFP to P22-StAv particles

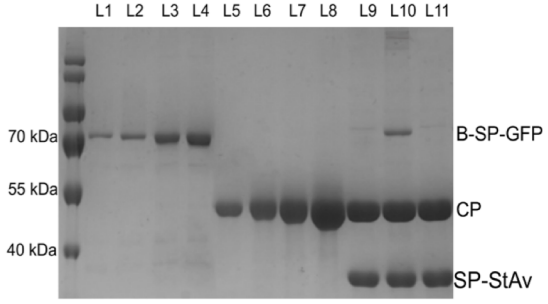

Figure S10. SDS-PAGE analysis of B-SP-GFP standards (L1: 2.5 pmol, L2: 5 pmol, L3: 10 pmol, L4: 15 pmol), CP standards (L5: 10 pmol, L6: 30 pmol, L7: 50 pmol, L8: 75 pmol), P22-StAv (L9), P22-StAv-B-SP-GFP (L10), and P22-StAv-I-SP-GFP (L11). Line scan densitometric profiles were generated for each of these lanes, as shown before. Using calibration curves, the number of bound copies of B-SP-GFP were calculated.

Electronic supplementary information

Dynamic light scattering of P22-StAv and P22-StAv-B-SP-GFP

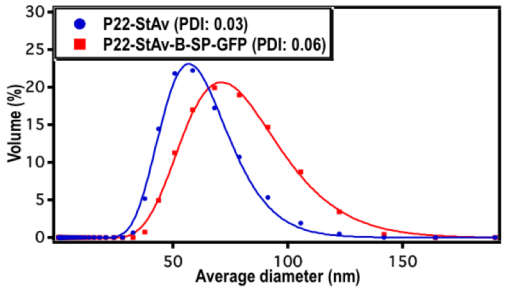

Figure S11. Dynamic light scattering revealed average particle size of 62.26 nm (PDI: 0.06, red trace) for P22-StAv-B-SP-GFP, and 60.31 nm (PDI: 0.03, blue trace) for P22-StAv, suggesting an increase in size due to bound B-SP-GFP on the exterior.

Immunodot-blot to investigate exterior decoration of P22-StAv with GFP

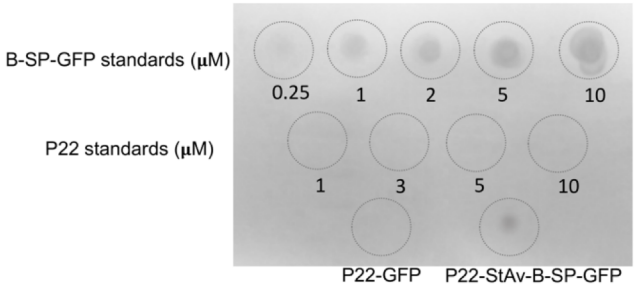

Figure S12. Immunoblot analysis confirms exterior functionalization of P22-StAv. Top row, B-SP-GFP standards were applied between 0.25 -10 μM concentration range. Middle row, P22 standards were spotted between 1 to 10 μM range. Last row, negative control (P22-GFP) and sample (P22-StAv-B-SP-GFP) was applied. The amount of P22-GFP and P22-StAv-B-SP-GFP applied on nitrocellulose membrane was normalized with respect to GFP concentration of 0.5 μM. The presence of dark spot in P22-StAv-B-SP-GFP and absence of a similar spot in P22-GFP indicates that GFP is exposed on the surface of capsid.

Calculation for determining concentration of StAv in P22

The concentration of StAv in P22 VLPs was calculated using molar mass provided by SEC-MALS. To get the number of StAv copies encapsulated in the P22 VLPs, the molar mass of empty coat protein shell (19.7 MDa) was subtracted from the molar mass of P22-StAv (31.6 MDa). The mass obtained was then divided by the theoretical molecular weight of StAv-SP, to give 338 copies of streptavidin per capsid. Using the number of copies and A280, the concentration of StAv was calculated as follows:

The total absorbance from P22-StAv can be written as follows

$A_T = A_{CP} + A_{StAv\text{-}SP}$.....(1)

Electronic supplementary information

where A_T is the total absorbance, A_{CP} is the absorbance contribution from CP, and $A_{StAv\text{-}SP}$ is the absorbance from StAv-SP. According to the Lambert-beer's law

$A_T = C_{CP}\,\varepsilon_{CP}\,l + C_{StAv\text{-}SP}\,\varepsilon_{StAv\text{-}SP}\,l$……..(2)

Where C_{CP} and $C_{StAv\text{-}SP}$ are the concentrations of CP and StAv-SP, respectively, ε_{CP} and $\varepsilon_{StAv\text{-}SP}$ are the extinction coefficients of CP and StAv-SP, respectively, and l is the path length of the cuvette. The concentration of CP in relation to StAv-SP, as determined by MALS, can be described by the equation:

$C_{CP} = 1.25 * C_{StAv\text{-}SP}$……..(3)

Therefore, equation 3 allows replacement of C_{CP} in equation 2 to give:
$A_T = 1.24 * C_{StAv\text{-}SP}\,\varepsilon_{CP} + C_{StAv\text{-}SP}\,\varepsilon_{StAv\text{-}SP}$…… (4)

In this equation, both extinction coefficients are known (calculated from expasy), the path length is known, and A_T is measured, leaving only $C_{StAv\text{-}SP}$. From equation 4 the concentration of StAv-SP was calculated under denatured conditions. The concentration calculated under denatured condition was used to calculate the extinction coefficient of the capsid containing 338 copies of streptavidin under non-denaturing condition. The extinction coefficient obtained was 215,000 $M^{-1}\,cm^{-1}$. This extinction was used to calculate the concentration of streptavidin for each sample used from the same capsid batch.
The extinction coefficient was calculated for every batch of P22-StAv prepared fresh, using the above protocol.

Nucleotide and amino acid sequences

6xhis-$StAv_{15\text{-}159}$-GAAG-ENLYFQS-GAAG-$SP_{142\text{-}303}$ (StAv-SP)

Nucleotide sequence

ATG GGT CAT CAT CAT CAT CAT CAT GCC GGC ATC ACC GGC ACC TGG TAC AAC CAG CTC GGC TCG ACC TTC ATC GTG ACC GCG GGC GCC GAC GGC GCC CTG ACC GGA ACC TAC GAG TCG GCC GTC GGC AAC GCC GAG AGC CGC TAC GTC CTG ACC GGT CGT TAC GAC AGC GCC CCG GCC ACC GAC GGC AGC GGC ACC GCC CTC GGT TGG ACG GTG GCC TGG AAG AAT AAC TAC CGC AAC GCC CAC TCC GCG ACC ACG TGG AGC GGC CAG TAC GTC GGC GGC GCC GAG GCG AGG ATC AAC ACC CAG TGG CTG CTG ACC TCC GGC ACC ACC GAG GCC AAC GCC TGG AAG TCC ACG CTG GTC GGC CAC GAC ACC TTC ACC AAG GTG AAG CCG TCC GCC GCC TCC ATC GAC GCG GCG AAG AAG GCC GGC GTC AAC AAC GGC AAC CCG CTC GAC GCC GTT CAG CAG GGT GCA GCA GGT GAA AAC CTG TAT TTC CAG AGC GGT GCG GCA GGC CGC AGC AAT GCC GTA GCA GAA CAG GGC CGC AAG ACT CAG GAG TTT ACC CAG CAA TCA GCG CAA TAC GTC GAA GCT GCC CGC AAA CAC TAT GAC GCG GCG GAA AAG CTC AAC ATC CCT GAC TAT CAG GAG AAA GAA GAC GCA TTT ATG CAA CTG GTT CCG CCT GCG GTT GGG GCC GAC ATT ATG CGC CTG TTC CCG GAA AAG TCC GCC GCG CTC ATG TAT CAC CTG GGG GCA AAC CCG GAG AAA GCC CGC CAG TTA CTG GCG ATG GAT GGG CAG TCC

Electronic supplementary information

GCG CTG ATT GAA CTC ACT CGA CTA TCC GAA CGC TTA ACT CTC AAG CCT CGC GGT AAA CAA ATC TCT TCC GCT CCC CCT GCT GAC CAG CCT ATT ACC GGT GAT GTC AGC GCA GCA AAT AAA GAT GCC ATT CGT AAA CAA ATG GAT GCT GCT GCG AGC AAG GGA GAT GTG GAA ACC TAC CGC AAG CTA AAG GCA AAA CTT AAA GGA ATC CGA TAA

Amino acid sequence

MGHHHHHHAGITGTWYNQLGSTFIVTAGADGALTGTYESAVGNAESRYVLTGRYDSAPATDGSGTALGW
TVAWKNNYRNAHSATTWSGQYVGGAEARINTQWLLTSGTTEANAWKSTLVGHDTFTKVKPSAASIDAAKK
AGVNNGNPLDAVQQGAAGENLYFQSGAAGRSNAVAEQGRKTQEFTQQSAQYVEAARKHYDAAEKLNIPD
YQEKEDAFMQLVPPAVGADIMRLFPEKSAALMYHLGANPEKARQLLAMDGQSALIELTRLSERLTLKPRGKQ
ISSAPPADQPITGDVSAANKDAIRKQMDAAASKGDVETYRKLKAKLKGIR

Cys-6xhis-$SP_{142\text{-}303}$-GGGGG-ENLYFQS-GGGGG-GFP (Cys-6xhis-SP-GFP)

Nucleotide sequence

ATG GGC TGC CAT CAT CAC CAC CAT CAC AGC ATG GAA CCA ACC ACC GAA ATT CAG GCA ACT GAA GAC TTA ACC CTG TCC GGC GAT CAT GCA GCG GCA TCT GCT GAT AGC TTA GTT GTC GAT AAT GCC AAC GAC AAT GCA GGT CAG GAA GAG GGC TTT GAG ATT GTC CTG AAG GAC GAT GAG ACA GCA CCA AAA CAA GAC CCG GCA AAG AAC GCA GAA TTC GCC CGC CGC CGC ATC GAG CGC AAA CGA CAG CGC GAG CTT GAG CAG CAG ATG GAG GCA GTT AAA CGC GGA GAA TTG CCG GAG AGT TTA CGG GTA AAC CCT GAC CTT CCT CCT CAG CCA GAC ATT AAC GCC TAT CTG TCA GAA GAA GGC CTG GCT AAA TAT GAC TAC GAC AAC AGC CGT GCG CTT GCC GCT TTC AAT GCT GCT AAT ACC GAA TGG CTA ATG AAA GCG CAG GAC GCC CGC AGC AAT GCC GTA GCA GAA CAG GGC CGC AAG ACT CAG GAG TTT ACC CAG CAA TCA GCG CAA TAC GTC GAA GCT GCC CGC AAA CAC TAT GAC GCG GCG GAA AAG CTC AAC ATC CCT GAC TAT CAG GAG AAA GAA GAC GCA TTT ATG CAA CTG GTT CCG CCT GCG GTT GGG GCC GAC ATT ATG CGC CTG TTC CCG GAA AAG TCC GCC GCG CTC ATG TAT CAC CTG GGG GCA AAC CCG GAG AAA GCC CGC CAG TTA CTG GCG ATG GAT GGG CAG TCC GCG CTG ATT GAA CTC ACT CGA CTA TCC GAA CGC TTA ACT CTC AAG CCT CGC GGT AAA CAA ATC TCT TCC GCT CCC CAT GCT GAC CAG CCT ATT ACC GGT GAT GTC AGC GCA GCA AAT AAA GAT GCC ATT CGT AAA CAA ATG GAT GCT GCT GCG AGC AAG GGA GAT GTG GAA ACC TAC CGC AAG CTA AAG GCA AAA CTT AAA GGA ATC CGA GGC GGC GGT GGT GGC GAA AAC CTG TAT TTC CAG AGC GGT GGC GGT GGC GGT ATG GTG AAG GGG GTG AAG GAA GTA ATG AAG ATC AGT CTG GAG ATG GAC TGC ACT GTT AAC GGC GAC AAA TTT AAG ATC ATT GGG GAT GGA ACA GGA GAA CCT TAC GAA GGA ACA CAG ACT TTA CAT CTT ACA GAG AAG GAA GGC AAG CCT CTG ACG TTT TCT TTC GAT GTA TTG ACA CCA GCA TTT CAG TAT GGA AAC CGT ACA TTC ACC AAA TAC CCA GGC AAT ATA CCA GAC TTT TTC AAG CAG ACC GTT TCT GGT GGC GGG TAT ACC TGG GAG CGA AAA ATG ACT TAT GAA GAC GGG GGC ATA AGT AAC GTC CGA AGC GAC ATC AGT GTG AAA GGT GAC TCT TTC TAC TAT AAG ATT CAC TTC ACT GGC GAG TTT CCT CCT CAT GGT CCA GTG ATG CAG AGG AAG ACA GTA AAA TGG GAG CCA TCC ACT GAA GTA ATG TAT GTT GAC GAC AAG AGT GAC GGT GTG CTG AAG GGA GAT GTC AAC ATG GCT CTG TTG CTT AAA GAT GGC CGC CAT TTG AGA GTT GAC TTT AAC ACT TCT TAC ATA CCC AAG AAG AAG GTC GAG AAT ATG CCT

Electronic supplementary information

GAC TAC CAT TTT ATA GAC CAC CGC ATT GAG ATT CTG GGC AAC CCA GAA GAC AAG CCG GTC AAG CTG TAC GAG TGT GCT GTA GCT CGC TAT TCT CTG CTG CCT TAA

Amino acid sequence

MGCHHHHHHSMEPTTEIQATEDLTLSGDHAAASADSLVVDNANDNAGQEEGFEIVLKDDETAPKQDPAK
NAEFARRRIERKRQRELEQQMEAVKRGELPESLRVNPDLPPQPDINAYLSEEGLAKYDYDNSRALAAFNAAN
TEWLMKAQDARSNAVAEQGRKTQEFTQQSAQYVEAARKHYDAAEKLNIPDYQEKEDAFMQLVPPAVGAD
IMRLFPEKSAALMYHLGANPEKARQLLAMDGQSALIELTRLSERLTLKPRGKQISSAPHADQPITGDVSAANK
DAIRKQMDAAASKGDVETYRKLKAKLKGIRGGGGGGENLYFQSGGGGGMVKGVKEVMKISLEMDCTVNGD
KFKIIGDGTGEPYEGTQTLHLTEKEGKPLTFSFDVLTPAFQYGNRTFTKYPGNIPDFFKQTVSGGGYTWERKM
TYEDGGISNVRSDISVKGDSFYYKIHFTGEFPPHGPVMQRKTVKWEPSTEVMYVDDKSDGVLKGDVNMALL
LKDGRHLRVDFNTSYIPKKKVENMPDYHFIDHRIEILGNPEDKPVKLYECAVARYSLLP

1. M. J. Waner and D. P. Mascotti, *Journal of biochemical and biophysical methods*, 2008, **70**, 873-877.
2. N. Humbert, A. Zocchi and T. R. Ward, *Electrophoresis*, 2005, **26**, 47-52.